ELSEVIER

Polymer 42 (2001) 757–764

polymer

www.elsevier.nl/locate/polymer

Dynamic interfacial properties of polymer blends under large step strains: shape recovery of a single droplet

R. Hayashi[a], M. Takahashi[a,*], H. Yamane[b], H. Jinnai[a], H. Watanabe[c]

[a]*Department of Polymer Science and Engineering, Kyoto Institute of Technology, Sakyo-ku, Kyoto 606-8585, Japan*
[b]*Division of Advanced Fibro Science, Graduate School, Kyoto Institute of Technology Sakyo-ku, Kyoto 606-8585, Japan*
[c]*Institute for Chemical Research, Kyoto University, Uji, Kyoto 611-0011, Japan*

Received 3 August 1999; received in revised form 11 January 2000; accepted 8 May 2000

Abstract

We observed shape recovery of a deformed droplet in an immiscible polymer matrix under large step strains using stereo microscopes from two directions. On application of a large step strain, a soft spherical droplet in a matrix with higher viscosity deformed to a flat ellipsoid. The stretch ratio of major axis of the flat ellipsoid was 5/4 times larger than that predicted from the affine deformation. The flat ellipsoid changed into a rod-like shape and then to a dumbbell, to an ellipsoid of revolution, and finally back to the sphere. The orientation angle between the major axis and shear direction did not change during the course of this shape recovery and was independent of the initial radius of the droplet. The time needed for the whole shape recovery got longer as the initial radius and the strain were increased. For a given step strain, the normalized interfacial area plotted against the stretch ratio fell onto a master curve irrespective of the initial radius of the undeformed droplet. It is shown that the deformed droplet reforms to the sphere after it passes through various shapes by reducing the interfacial area. © 2000 Elsevier Science Ltd. All rights reserved.

Keywords: Immiscible polymer blend; Step strain; Shape recovery of droplet

1. Introduction

A considerable number of studies [1–10] have been carried out on rheology and structures of immiscible polymer blends to describe the rheological properties in terms of the interface related quantities. Scholts et al. [3] found that a recovery time for a droplet deformation evaluated from microscopy was close to the viscoelastic terminal relaxation time of blends after cessation of steady shear flow. Palierne [4,5] proposed the emulsion model, which predicts the linear viscoelastic behavior of blends. In this model, deformation of droplets by an applied shear field and recovery due to the interfacial tension lead to the terminal relaxation. Good applicability [6–10] of the Palierne model has been found in many blends, especially in blends comprising dispersed droplet phases.

In terms of dynamic interfacial properties, the interfacial tension is one of the essential factors for understanding mechanical properties and the morphology of polymeric blends. If a droplet is highly extended under a certain flow field or a fiber is embedded in a matrix of another polymer, the capillary instability results in sinusoidal distortions in the interface of a liquid cylinder. Following the well-known experiments and analyses by Rayleigh [11] and Tomotika [12] on viscous materials, studies [13–20] related to the interfacial properties of viscoelastic polymeric materials have been carried out. Elemans et al. [13] proposed a method to measure the interfacial tension for immiscible polymer blends, known as the breaking thread method, based on the Tomotika's analysis. In conventional methods, such as the pendant drop method, it is difficult to determine whether the equilibrium is attained, since this method relies on the balance between gravitational force and the interfacial tension. Cohen and Carriere [15–17] introduced a novel method, known as the imbedded fiber retraction method, in which the interfacial tension is evaluated from changes in the shape of a short fiber of one polymer embedded in another polymer into a final spherical shape. Moreover, according to other recent papers [18–20], the interfacial tension between the coexisting phases in polymer blends can also be estimated from the droplet shape under shear flow and recovery of the droplet shape after the cessation of shear flow. However, it is still unclear how the interfacial tension and the droplet/matrix viscoelasticity correlate with the shape recovery of the droplet.

* Corresponding author. Tel.: +81-75-724-7835; fax: +81-75-724-7800.
E-mail address: mdt@ipc.kit.ac.jp (M. Takahashi).

0032-3861/01/$ - see front matter © 2000 Elsevier Science Ltd. All rights reserved.
PII: S0032-3861(00)00373-6

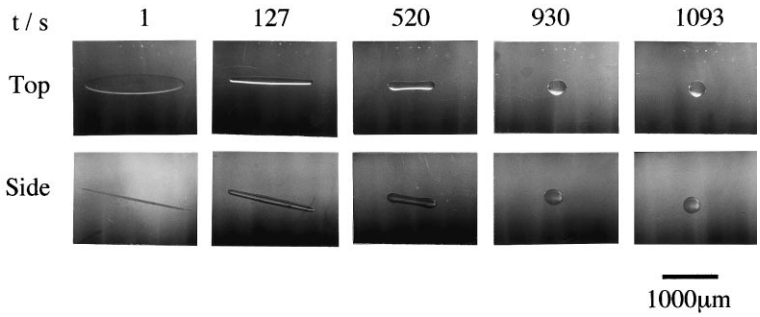

Fig. 1. A set of microphotos of a poly(isobutylene) droplet ($\eta_d = 60$ Pa s, $r_0 = 160$ μm) in a poly(dimethyl siloxane) ($\eta_m = 900$ Pa s) during the shape recovery after the application of a large step strain $\gamma = 5$. The top and side views are shown.

On the other hand, since Taylor's pioneering work, [21,22] many studies [23–29] have been carried out to observe the droplet deformation and shape recovery in various flow fields. Delaby et al. [23–25] examined the deformation of a droplet under uniaxial elongational flow by quenching the sample. They reported that the deformation of the droplet in a polymeric matrix strongly depended on the viscosity ratio of the droplet to the matrix. In particular, Delaby et al. found that the soft droplet in a very viscous matrix deformed considerably more than expected from the affine deformation. Mighri et al. [26] reported on the contribution of the droplet/matrix elasticity to the deformation of a single droplet suspended in the medium under the uniaxial elongational flow along the central axis of a converging conical channel made of Plexiglas. Levitt et al. [27] developed a device, that had two counter-rotated transparent disks to generate a simple shear flow. The shape of the droplets, which was produced after a fiber embedded between two disks broke-up due to the capillary instability, was observed in the melt-state. However, measurements of the deformed droplet under the simple shear flow were rather qualitative because only the top view of the droplet was observed. Moreover, the droplet curved owing to the rotating parallel disks.

Fundamental understanding of the deformation/recovery and breakup mechanisms of an isolated polymer droplet under the deformation fields is essential to correlate the droplet deformation with rheology in polymer blends. The step-strain experiment is the simplest way to study these deformation/recovery behaviors. In this experiment, droplets in polymer blends deform instantaneously and the shape recovery (or relaxation) of the droplet is traced. On the other hand, under steady flows, the droplet shape is observed with some recovery of the droplets depending on the strain rate and a competition between the deformation and the recovery of the droplets determine this shape. The droplet shapes under the shear flows have recently been reported by many researchers [30–36]. However, to our best knowledge, there have been only one report [37] on the droplet shape recovery under the step shear strain.

In our previous study [37], we observed the deformation and shape recovery of an isolated droplet from two directions, i.e. side and top directions, after the application of large step shear strains. The effect of the applied strain on the shape recovery was examined. Therefore, the total recovery time strongly depended on the magnitude of the applied strain. However, we have not yet examined the effect of the droplet size on the shape recovery. Measurements and evaluation of the interfacial area are also very important to consider the mechanism of shape recovery. The objectives of the present study are the following: direct observation of the shape of droplets with various initial radii for (1) accurate determination of the time dependence of the droplet dimensions and orientation; (2) investigation into the dependence of shape recovery time on the initial radius; and (3) evaluation of the interfacial area during the course of shape recovery and consideration of the recovery mechanism.

2. Experimental

The component polymers are poly(isobutylene) (PIB from Polysciences. Inc.) and poly(dimethyl siloxane) (PDMS from Shin-Etsu Chemical Co., Ltd). Dynamic mechanical measurements were carried out using the Bohlin Rheometer CSM in a parallel-plate geometry (12.5 mm radius, 1 mm gap). Frequency dependences of the storage modulus G' and the absolute value of complex viscosity $|\eta^*|$ of the polymers measured at 23°C are shown in our previous paper [37]. The zero shear viscosities of PIB (η_d) and PDMS (η_m) at 23°C is 60 and 900 Pa s, respectively. The viscosity ratio $K(=\eta_d/\eta_m)$ is 0.067 and the elasticity ratio $K'(=\eta_d J_{ed}/\eta_m J_{em})$ is 9.62×10^{-4}, where J_e is the steady state compliance and subscripts d and m denote droplet and matrix, respectively.

The apparatus used for the observation of PIB droplets in the PDMS matrix is described elsewhere [37]. Before the experiments, the PDMS sample was kept in vacuum oven overnight at room temperature to eliminate air bubbles. Then, a small amount of PIB (0.1–0.2 μl) was injected into the PDMS matrix with a microsyringe to make a PIB droplet. The process of deformation and shape recovery of the droplet in the PDMS matrix was observed at room

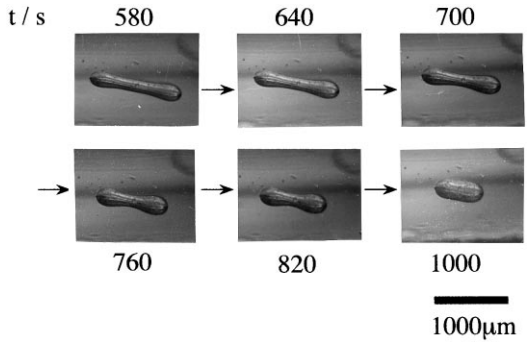

Fig. 2. Microphotos of a poly(isobutylene) droplet ($r_0 = 230$ μm) at $\gamma = 5$ in the process from the dumbbell shape to the ellipsoid of revolution. The side view is shown.

temperature from top and side by using two stereo-microscopes equipped with photographic and/or CCD cameras.

3. Results and discussion

3.1. Observation of time change of the deformed droplet

The droplet with the initial radius r_0, in the range of 140–280 μm, were subjected to the step strains $\gamma(\leq 5)$. The droplets with $r_0 = 160$ and 280 μm were examined only for $\gamma = 5$. In the previous paper [37], we reported that the shapes of the PIB droplet ($r_0 = 230$ μm) during the course of the shape recovery strongly depended on γ.

Fig. 1 shows a series of photographs of the droplet with $r_0 = 160$ μm at $\gamma = 5$ taken at various stages of shape recovery. The photographs were taken from top and side of the apparatus. Immediately after the deformation, the droplet shape is a flat ellipsoid. This deformed droplet gradually changes into a rod-like shape. After the recovery from the flat ellipsoid to the rod-like shape, the droplet becomes symmetrical around the major axis. The increase in the diameter is more prominent at the droplet ends than at the center, resulting in a dumbbell shape (having bulbs at the ends). Finally, the droplet changes into an ellipsoid of revolution and back to the sphere with its original radius, r_0.

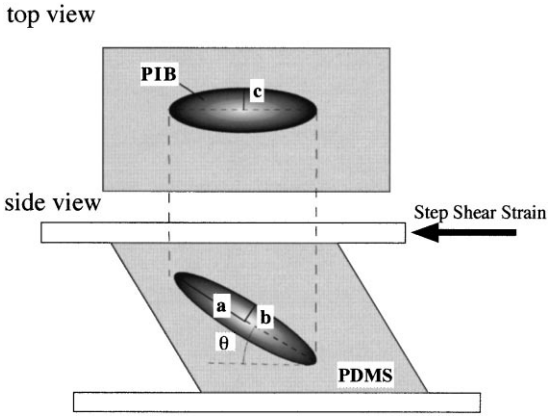

Fig. 3. Definition of the dimensions of the deformed droplet along three principal axes and the orientation angle θ.

Fig. 2 shows detailed changes from the dumbbell shape to the ellipsoid of revolution in the case of $r_0 = 230$ μm at $\gamma = 5$. The dumbbell does not break up at the center and soon becomes the ellipsoid of revolution, although the bulb diameter increases with time.

We have also observed the breakup of the droplet with $r_0 = 170$ μm. The magnitude of the attainable strain without breakup is seven for the droplet. At the magnitude of the applied strain $\gamma = 8$, the droplet first changes into a long rod-like shape, and then the droplet breaks up into some smaller droplets due to the capillary instabilities [11,12] appearing on the cylindrical interface. The length of the droplet decreases somewhat during this process. Stone and Leal [38] examined the mechanism of the recovery and breakup of a long extended droplet suspended in other matrix by the numerical simulations. They demonstrated that the dynamical evolution of the droplet shape depends on the viscosity ratio and the initial droplet shape, in case that both ends have the bulbous or pointed shape. Tjahjadi et al. [39] investigated the droplet breakup using the results of simulations by Stone and Leal [38] and showed that the experimental results examined in Couette flow are in agreement with the simulations. Our results of the time evolution of the droplet breakup are similar to those of Tjahjadi et al. This may be due to the coincidence of the viscosity ratio $K = 0.067$ in both systems.

3.2. Measurement of size and orientation of the deformed droplet

Dimensions of the deformed droplet are defined in Fig. 3. The dimensions along the major and two minor axes are denoted as a, b and c and an orientation angle is defined as θ. In case of the dumbbell, b and c are taken as the radius of the central part. Fig. 4 summarizes the time dependence of θ for the deformed droplets with various r_0 after the application of the step strain γ (as indicated in Fig. 4). Since the rotational relaxation time of the droplets (with $r_0 \geq 140$ μm) in the viscous PDMS matrix ($\eta_m = 900$ Pa s) is extremely long (estimated to be $\sim 10^{13}$ s) [37], θ stays almost constant during the shape recovery. In Fig. 4, the horizontal dashed lines indicate the orientation angle θ_a of the strain ellipsoid

$$\theta_a = \tfrac{1}{2} \cot^{-1}\left(\frac{\gamma}{2}\right), \tag{1}$$

which is equal to the orientation angle for affine deformation. At $\gamma = 3$ and 5, θ agrees with θ_a, although θ at $\gamma = 1$, 2 and 4 appears to be slightly larger than θ_a.

In Fig. 5, principal stretch ratios of the droplet, a/r_0, b/r_0 and c/r_0, are plotted against time after the application of strain of $\gamma = 5$ for two droplets with $r_0 = 140$ and 280 μm. Just after the application of the step strain, b/r_0 is much smaller than c/r_0 (~ 1), and thus the droplet takes a flat

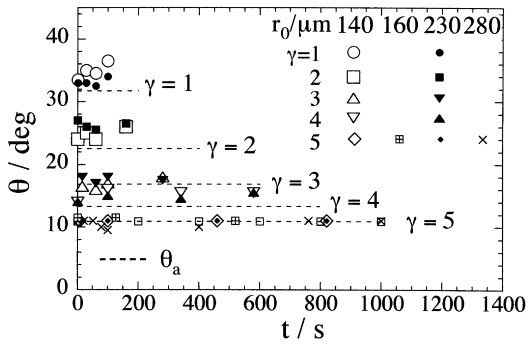

Fig. 4. Time dependences of the orientation angle θ for the droplets with various initial radii after the application of various strains. The broken line indicates the orientation angle for the affine deformation θ_a at each strain.

ellipsoidal shape. The three stretch ratios stay almost constant for a short period of time ($t < 10$ s). With time t up to ca. 100 s, c/r_0 decreases while b/r_0 increases, resulting in a rod-like shape of the droplet having $c/r_0 \cong b/r_0$. Then, a/r_0 begins to decrease slowly and the droplet reforms to a dumbbell. Finally, the droplet changes into an ellipsoid of revolution, and the three stretch ratios rapidly approached unity to recover the spherical shape. Clearly, the whole recovery time depends on the initial radius of the droplet.

It is interesting to compare the droplet stretch ratio a/r_0 (just after the application of the step strain) with the principal stretch λ_1 of the strain ellipsoid

$$\lambda_1 = \sqrt{1 + \frac{\gamma^2}{2} + \frac{\gamma}{2}\sqrt{4 + \gamma^2}}. \tag{2}$$

Fig. 6 shows a/r_0 as a function of λ_1 for droplets with various r_0. The stretch ratio a/r_0 is found to be 5/4 times larger than the principal stretch λ_1. Similar results were obtained in experiments under elongational flow in immiscible polymer blends [23,26]. Delaby et al. [23] experimentally found that the droplet deformation was different from the matrix deformation in the uniaxial elongational flow. This difference depends on the droplet/matrix viscosity ratio. They suggested that the deformation in the vicinity

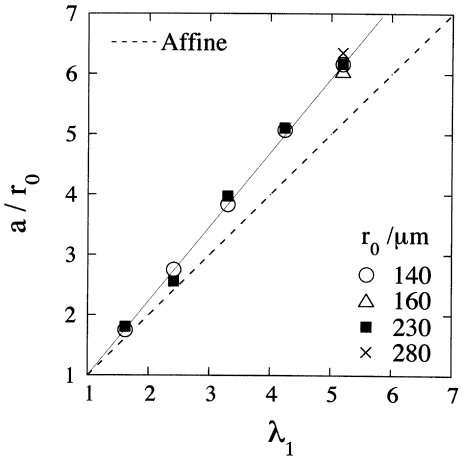

Fig. 6. The stretch ratio a/r_0 of droplets just after the application of step strain plotted against the principal stretch of the strain ellipsoid.

of the droplet ends along the elongational direction was smaller than that of the surrounding matrix, whereas the deformation in the vicinity of droplet sides was larger. Based on the emulsion model of Palierne, Delaby et al. derived the following equation:

$$\frac{\lambda_d - 1}{\lambda_1 - 1} = \frac{5}{2K + 3}, \tag{3}$$

where λ_d and K are a/r_0 and the viscosity ratio, respectively. When K is small, $(\lambda_d - 1)/(\lambda_1 - 1)$ approaches 5/3, however, 5/4 is observed for our system. Elasticity effect is important to consider the droplet deformation. Mighri et al. [26] examined the contribution of elasticity to the droplet deformation for immiscible polymer blends with weak elasticity (solution sample). Although their solution samples have the same viscosity ratio ($K = 0.63$) as the polymer melt blends studied by Delaby et al. [23], the droplet deformation is much smaller. The relationship between the droplet and matrix deformation is much more complicated than Eq. (3). Mighri et al. concluded that the droplet deformation was affected not only by K but also by the elasticity

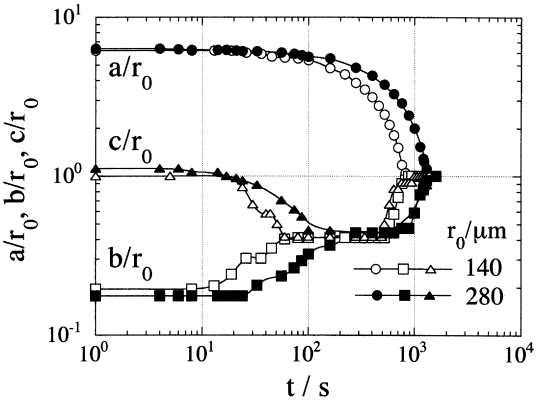

Fig. 5. Time dependences of the three principal stretch ratios of the droplets at $\gamma = 5$.

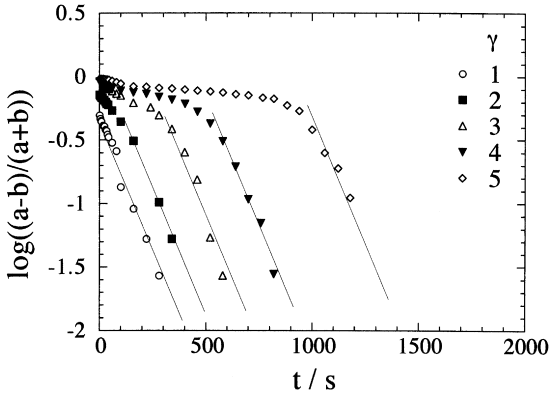

Fig. 7. Semi-log plot of the droplet deformation $(a - b)/(a + b)$ against time obtained at various strains for the droplet with $r_0 = 230$ μm.

Table 1
Characteristic times τ_{ES} and τ_{FR} for droplet shape recovery and the viscoelastic relaxation time τ_D from the emulsion model by Palierne

	τ_{FR} (s)	τ_{ES} (s)		τ_D (s)
r_0 (μm)	$\ln(c/r_0)$	$\ln(a/r_0)$	$(a-b)/(a+b)$	Emulsion model (Palierne)
140	15.8	60.0	67.0	51.5
230	28.2	105	108	84.5
280	31.0	120	125	103

ratio K', the droplet/matrix interfacial tension and magnitude of shear thinning [26].

3.3. Evaluation of relaxation times

The droplet deformation is expressed by the Hencky type strain $\ln(a/r_0)$ or by the classical strain $(a-b)/(a+b)$. Fig. 7 shows the plots of $\log[(a-b)/(a+b)]$ against time obtained at various strains for the droplet ($r_0 = 230$ μm). The whole recovery of droplet deformation is not represented by a single exponentially decay process, as shown clearly for $\gamma = 2$–5. However, at the late stage of shape recovery, $\log[(a-b)/(a+b)]$ at each strain is represented by a strain line, i.e. $(a-b)/(a+b) \sim \exp(-t/\tau_{ES})$. The slopes of the straight lines are almost the same from which we evaluate a relaxation time τ_{ES} to be ca. 108 s. This means that the droplet recovers to the spherical shape (at the late stage) in the same dynamical way irrespective of γ. The time τ_{ES} corresponds to the recovery time for the droplet shape from the ellipsoid of revolution (E) to the sphere (S). Semilog plots of $\ln(a/r_0)$ against t give a similar value of τ_{ES} (~105 s) [37].

In the emulsion model [4,5], a viscoelastic relaxation time of a dispersed phase in an immiscible polymeric matrix is associated with the deformation and shape recovery of the droplet in linear viscoelastic region

$$\tau_D = \frac{\eta_m r_0}{4\alpha} \frac{(19K+16)[2K+3-2\phi(K-1)]}{10(K+1)-2\phi(5K+2)} \quad (4)$$

Here, α and ϕ are the interfacial tension and the volume fraction of the dispersed phase, respectively. For a single droplet, τ_D is obtained by putting $\phi \to 0$. The α value in our system is experimentally found to be 3.1 mN/m [40] from the pendant drop method [41,42]. Table 1 compares the calculated τ_D with the experimental time τ_{ES} for the droplets at various r_0. The time τ_{ES} shows fair agreement with τ_D. We note that τ_{ES} is proportional to r_0 as expected from the Palierne theory.

In Fig. 8, the stretch ratios a/r_0, b/r_0 and c/r_0 shown in Fig. 5 are replotted against a reduced time t/τ_{ES}. The data in the late stage (IV), representing the change from the ellipsoid of revolution to the sphere fell almost onto a universal curve. More interestingly, the data in the earlier stage showing the change from the flat ellipsoid (I) to the rod-like shape (II) can also be scaled by t/τ_{ES}. This indicates that the short time

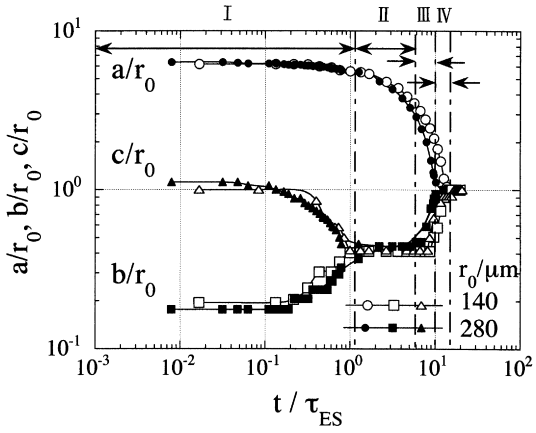

Fig. 8. The three principal stretch ratios of the droplets as functions of the normalized time t/τ_{ES}. The shape of the droplets are: (I) ellipsoid; (II) rod-like; (III) dumbbell; and (IV) ellipsoid of revolution.

constant has the same r_0 dependence as τ_{ES}. Let us call this short time constant as τ_{FR}. Since b/r_0 is very small in the earlier stage and may include considerable uncertainty, we evaluate τ_{FR} from the plots of $\log[\ln(c/r_0)]$ vs. t. The evaluated τ_{FR} at each r_0 is shown in Table 1.

3.4. Time constants in the stress relaxation

In the previous section, τ_{ES} was found to have a similar value to the calculated τ_D. However, τ_D obtained from the emulsion model corresponds to the viscoelastic relaxation time, while τ_{ES} characterizes the shape recovery. Therefore, it is necessary to clarify the relationship between τ_{ES} and τ_D. To this end, we compare the shear stress $\sigma_{xy}^{(i)}$ due to the interfacial tension and some structural parameters specifying the droplet deformation.

The $\sigma_{xy}^{(i)}$ is given by [43–45]

$$\sigma_{xy}^{(i)} = -\left(\frac{\alpha}{V}\right)\int_{\text{surface}} n_x n_y \, dS \quad (5)$$

where n_x and n_y are the x and y components of the unit vector normal to the interface, and V is the volume of the system. We consider monodisperse liquid droplets whose shape is the ellipsoid of revolution. The droplets are dilutely dispersed in the system and not interacting with each other. The major and minor axes of the droplet are defined as $a = \lambda r_0$ and $b = \lambda^{-1/2} r_0$, with $\lambda(>1)$ being the stretch ratio, and r_0 is the radius of a sphere having the same volume as the droplet. If the major axis lies in the x–y plane and orients to the x-direction with an angle θ, Eq. (5) becomes

$$\sigma_{xy}^{(i)} = \left(\frac{3\alpha\phi}{8r_0}\right)\sin 2\theta \times\left[\frac{\lambda^3+2}{\lambda(\lambda^{3\prime}-1)} + \frac{\sqrt{\lambda}(\lambda^3-4)}{(\lambda^3-1)} \times \frac{\arcsin\sqrt{1-\lambda^{-3}}}{\sqrt{1-\lambda^{-3}}}\right]. \quad (6)$$

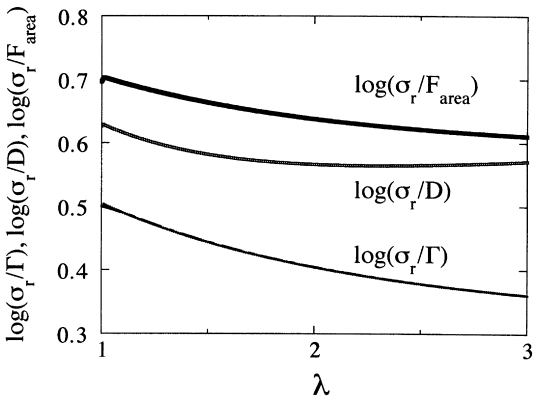

Fig. 9. The ratios of the normalized shear stress σ_r to the Hencky strain Γ, the extent of deformation D, and the normalized increment of the surface area F_{area} for the ellipsoid of revolution plotted against the droplet stretch ratio λ.

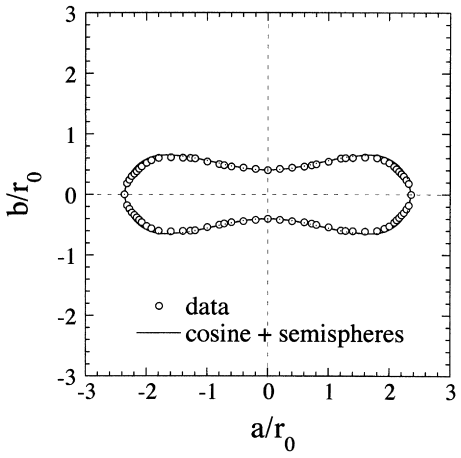

Fig. 10. The curve-fitting to the dumbbell profile obtained at 760 s after the application of the strain $\gamma = 5$.

where ϕ is the volume fraction of the droplets, $\phi = 4\pi r_0^3 \nu_d/3$ and ν_d is the number of the droplets per unit volume.

The surface area of the droplets per unit volume, S_E, is expressed as

$$S_E = 2\nu_d \pi r_0^2 \left[\frac{1}{\lambda} + \frac{\sqrt{\lambda}\arcsin\sqrt{1-\lambda^{-3}}}{\sqrt{1-\lambda^{-3}}} \right]. \quad (7)$$

From S_E, a square root of the normalized excess surface area is defined as:

$$F_{area} = \sqrt{\frac{S_E - S_0}{S_0}} \quad (8)$$

where $S_0 = 4\nu_d \pi r_0^2$ is the surface area of the undeformed droplets. Ratios of the normalized stress, $\sigma_r = 8r_0\sigma_{xy}^{(i)}/(3\alpha\phi \sin 2\theta)$, to the Hencky strain $\Gamma = \ln(a/r_0)$, the extent of deformation $D = (a-b)/(a+b)$ and F_{area} are plotted against the stretch ratio $\lambda(= a/r_0)$ in Fig. 9. As λ decreases, all these three ratios increase. This means that, as the droplet recovers to a sphere ($\lambda \rightarrow 1$), the reduction of σ_r is less significant than those of Γ, D and F_{area}. Thus, τ_D characterizing the relaxation of $\sigma_{xy}^{(i)}$ is somewhat longer than τ_{ES} that represents the decay of Γ and D. However, as shown in Fig. 9, the variations in σ_r/Γ, σ_r/D and σ_r/F_{area} are within 10% over the range of λ from 1.5 to 1, where the shape of the droplet in our system changes from an ellipsoid of revolution to a sphere. This λ range corresponds to the range where Γ and D can be expressed by an exponential function $\exp(-t/\tau_{ES})$ as shown in Fig. 7 and in our previous paper.

The above results mean that the interfacial stress $\sigma_{xy}^{(i)}$ and the droplet deformation parameters Γ and D decay at essentially the same rate in a terminal stage of relaxation after imposition of a step strain. In the Palierne theory, the terminal viscoelastic relaxation rate coincides with the relaxation rate of $\sigma_{xy}^{(i)}$. Thus, the observed τ_{ES} (specifying the decay of Γ and D) are in close agreement with the theoretical τ_D, as demonstrated in Table 1.

Concerning this result, we add a few comments about the stress components. In the theories by Bachelor [44] and Onuki [45], the stress *against step strain* includes an interfacial component ($\sigma_{xy}^{(i)}$) and the viscous component, the latter resulting from flow due to motion of the droplet/matrix interface. (The stress derived from the Palierne theory also includes the interfacial and viscous components, although the micro-structural expressions of these components are different from those in the theories of Bachelor and Onuki.) The relative magnitude of these components changes with the viscosities of the droplet and matrix, the droplet volume fraction, and the interfacial tension. However, both components decay on the recovery of the droplet shape to a sphere and have essentially the same relaxation time (in the terminal relaxation process). Thus, the coincidence of the structural relaxation time τ_{ES} and the viscoelastic relaxation time seen in Table 1 is also consistent with the theories of Bachelor and Onuki.

3.5. Evaluation of the surface area

The primary driving force for the shape recovery of the droplet may be the reduction of the droplet/matrix interfacial area. Therefore, it is interesting to examine the surface areas of a droplet in various shapes, i.e. the flat ellipsoid ($c = r_0$), the rod-like, the dumbbell, and the ellipsoid of revolution. The surface areas S and volumes V of the flat ellipsoid and the ellipsoid of revolution are geometrically well defined. However, we have to use the geometrically explicit models for evaluating S for the rod-like shape and the dumbbell: the rod-like shape is modeled as a cylinder with two semi-spheres at both ends, and the dumbbell as a revolution of a cosine curve with two semi-spheres at both ends [37]. The surface area of these models can be calculated under the condition of constant volume.

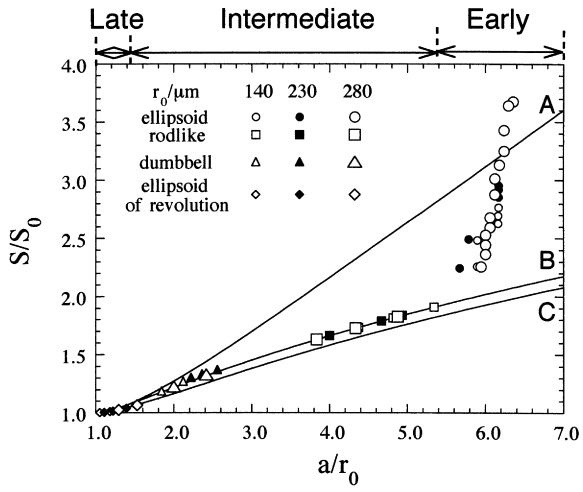

Fig. 11. The normalized surface area S/S_0 obtained for droplets with various initial radii as functions of the droplet stretch ratio a/r_0. The three lines indicate S/S_0 of: (A) the flat ellipsoid; (B) the cylinder + semi spheres; and (C) the ellipsoid of revolution.

For the dumbbell, S is given by [37]

$$S = 4\pi r^2 + 4\pi \int_0^l f(x)\left[1 + \left(\frac{\mathrm{d}f(x)}{\mathrm{d}x}\right)^2\right]^{1/2} \mathrm{d}x, \tag{9}$$

with

$$f(x) = \frac{r(1+\delta)}{2} - \frac{r(1-\delta)}{2}\cos\left(\frac{x}{l}\pi\right) \tag{10}$$

Here, $f(x)$ is a function describing the surface profile at the middle of the dumbbell. δ represents b/r with r being the radius of the semi spheres, and $2l$ represents the wavelength of the cosine curve. Fig. 10 shows the experimental data for the dumbbell ($r_0 = 230$ μm) at 760 s after the application of $\gamma = 5$. The solid line in the figure represents the best fit of the model as given by Eq. (10).

Fig. 11 shows the plots of normalized surface area S/S_0 against a/r_0 for the droplets with $r_0 = 140$, 230 and 280 μm after the application of the strain $\gamma = 5$. Here S_0 represents the surface area of the initial spherical droplet. Three lines in Fig. 11 represent S/S_0 of the flat ellipsoid (line A), the cylinder + semi spheres (line B), and the ellipsoid of revolution (line C) as functions of a/r_0 under the condition of the constant volume. The lines for the modeled dumbbell shape with various δ lie between line B and line C [37].

The observed reduction of S/S_0 due to the droplet shape recovery can be divided into the following three stages as shown in Fig. 11. During the early stage, the flat ellipsoid reduces its surface area remarkably by changing into the rod-like shape with very small reduction in a/r_0. The time constant for this stage, τ_{FR}, depends on r_0. During the intermediate stage, the droplet reduces the surface area mainly by contracting a/r_0. The change in the surface area due to the shape change (rod-like to dumbbell) is small in this stage. The droplet exhibits the dumbbell shape after it becomes the rod-like shape due to the capillary instability. In the late stage from the ellipsoid of revolution to the sphere, the droplet recovers to the spherical shape with the time constant τ_{ES} depending on r_0.

4. Conclusions

A PIB droplet embedded in a more viscous matrix of PDMS becomes a flat ellipsoid just after application of strain $\gamma > 4$ and changes into a rod-like shape, a dumbbell, an ellipsoid of revolution, and finally back to the sphere. During this recovery process, the orientation angle between major axis and shear direction stays unchanged and is close to that expected from the affine deformation. Just after application of the strain, the stretch ratio along the major axis, a/r_0, is independent of r_0 and is about 1.25 times greater than the value calculated for the affine deformation. The time constants for the shape change from the flat ellipsoid to the rod-like and from the ellipsoid of revolution to the sphere, τ_{FR} and τ_{ES}, can be evaluated from the plots of $\log(\ln(c/r_0))$ and $\log(\ln(a/r_0))$ vs. t, respectively. Both τ_{FR} and τ_{ES} are found to be proportional to r_0. The time τ_{ES} is comparable with τ_D, the viscoelastic relaxation time for the droplet given by the emulsion model. Plots of the normalized surface area against the stretch ratio of the droplets are almost independent of r_0 when the same strain is applied. At the early stage of the shape recovery, the large reduction of the surface area occurs by changing the shape from the flat ellipsoid to the rod-like without reducing the droplet stretch remarkably. At the intermediate stage, the further reduction occurs slowly by reducing the droplet stretch. The capillary instability appears at this stage but the reduction of the surface area due to this instability is small. At the late stage, the droplet recovers to the spherical shape with the time constant τ_{ES} depending on r_0.

Acknowledgements

The authors cordially thank Prof. Mitsunobu Kitamura for his help in the density measurement of our samples required for evaluation of the interfacial tension by the pendant drop method.

References

[1] Graebling D, Muller R. J Rheol 1990;34:193.
[2] Gramespacher H, Meissner J. J Rheol 1992;36:1127.
[3] Scholtz P, Froelich D, Muller R. J Rheol 1989;33:481.
[4] Palierne JF. Rheol Acta 1990;29:204.
[5] Palierne JF. Rheol Acta 1991;30:497.
[6] Graebling D, Muller R, Palierne JF. Macromolecules 1993;26:320.
[7] Brahimi B, Ait-Kadi A, Ajji A, Jerome R, Fayt R. J Rheol 1991;35:1069.
[8] Bousmina M, Muller R. J Rheol 1993;37:663.
[9] Bousmina M, Bataille P, Sapieha S, Schreiber HP. J Rheol 1995;39:499.

[10] Maeda S, Kamei E. J Soc Rheol Jpn 1994;22:145.
[11] Rayleigh L. Proc R Soc London 1879;29:71.
[12] Tomotika S. Proc R Soc London 1935;A150:322.
[13] Elemans PHM, Janssen JMH, Meijer HEM. J Rheol 1990;34:1311.
[14] Elmendorp JJ. Polym Engng Sci 1986;26:418.
[15] Carriere CJ, Cohen A, Arends CB. J Rheol 1989;33:681.
[16] Cohen A, Carriere CJ. Rheol Acta 1989;28:223.
[17] Carriere CJ, Cohen A, Arends CB. J Rheol 1991;35:205.
[18] Tjahjadi M, Ottino JM, Stone HA. AIChe J 1994;40:385.
[19] Luciani A, Champagne MF, Utracki LA. J Polym Sci Part B: Polym Phys 1997;35(9):1393.
[20] Sigillo I, Santo L, Guido S, Grizzuti N. Polym Engng Sci 1997; 37:1540.
[21] Taylor GI. Proc R Soc 1932;A138:41.
[22] Taylor GI. Proc R Soc 1934;A146:501.
[23] Delaby I, Ernst B, Germain Y, Muller R. J Rheol 1994;38:1705.
[24] Delaby I, Ernst B, Muller R. Rheol Acta 1995;34:525.
[25] Delaby I, Ernst B, Froelich D, Muller R. Polym Engng Sci 1996;36:1627.
[26] Mighri F, Ajji A, Carreau PJ. J Rheol 1997;41:1183.
[27] Levvit L, Macosko CW. Polym Engng Sci 1996;36:1647.
[28] Janssen JJM, Boon A, Agterof WGM. AIChe J 1994;40:1929.
[29] Janssen JJM, Boon A, Agterof WGM. AIChe J 1997;43:1436.
[30] Takahashi Y, Suzuki H, Nakagawa Y, Noda I. Polym Intl 1994;34:327.
[31] Kitade S, Ichikawa A, Imura N, Takahashi Y, Noda I. J Rheol 1997;41:1039.
[32] Vinckier I, Moldenaers P, Mewis J. J Rheol 1996;40:613.
[33] Vinckier I, Moldenaers P, Mewis J. J Rheol 1997;41:705.
[34] Vinckier I, Mewis J, Moldenaers P. Rheol Acta 1997;36:513.
[35] Grizzuti N, Bifulco O. Rheol Acta 1997;36:406.
[36] Guido S, Villone M. J Rheol 1998;42:395.
[37] Yamane H, Takahashi M, Hayashi R, Okamoto K, Kashihara H, Masuda T. J Rheol 1998;42:567.
[38] Stone HA, Leal LG. J Fluid Mech 1989;198:399.
[39] Tjahjadi M, Stone HA, Ottino JM. J Fluid Mech 1992;243:297.
[40] Hayashi R, Takahashi M, Yamane H. In preparation.
[41] Andreas JM, Hauser EA, Tucker WB. J Phys Chem 1938;42:1001.
[42] Demarquette NR, Kamal MR. Polym Engng Sci 1994;34:1823.
[43] Doi M, Ohta T. J Chem Phys 1991;95:1242.
[44] Batchelor GK. J Fluid Mech 1970;41:545.
[45] Onuki A. Europhys Lett 1994;28:175.